

# An Efficient Uplink Multi-Connectivity Scheme for 5G mmWave Control Plane Applications

Marco Giordani<sup>†</sup>, Marco Mezzavilla<sup>◇</sup>, Sundeep Rangan<sup>◇</sup>, Michele Zorzi<sup>†</sup>

<sup>†</sup> Department of Information Engineering (DEI), University of Padova, Italy

<sup>◇</sup>NYU Wireless, Brooklyn, NY, USA

{giordani, zorzi}@dei.unipd.it, {mezzavilla, srangan}@nyu.edu

## Abstract

The millimeter wave (mmWave) frequencies offer the potential of orders of magnitude increases in capacity for next-generation cellular systems. However, links in mmWave networks are susceptible to blockage and may suffer from rapid variations in quality. Connectivity to multiple cells – at mmWave and/or traditional frequencies – is considered essential for robust communication. One of the challenges in supporting multi-connectivity in mmWaves is the requirement for the network to track the direction of each link in addition to its power and timing. To address this challenge, we implement a novel uplink measurement system that, with the joint help of a local coordinator operating in the legacy band, guarantees continuous monitoring of the channel propagation conditions and allows for the design of efficient control plane applications, including handover, beam tracking and initial access. We show that an uplink-based multi-connectivity approach enables less consuming, better performing, faster and more stable cell selection and scheduling decisions with respect to a traditional downlink-based standalone scheme. Moreover, we argue that the presented framework guarantees (i) efficient tracking of the user in the presence of the channel dynamics expected at mmWaves, and (ii) fast reaction to situations in which the primary propagation path is blocked or not available.

## Index Terms

5G, millimeter wave, multi-connectivity, initial access, handover, blockage, beam tracking.

A preliminary version of this paper was presented at the *15th Annual Mediterranean Ad Hoc Networking Workshop (Med-Hoc-Net)*, Vilanova i la Geltru, Barcelona, Spain, June 2016 [1].

## I. INTRODUCTION

The millimeter wave (mmWave) bands – roughly above 10 GHz – have attracted considerable attention for meeting the ever more demanding performance requirements of micro and picocellular networks [2]. These frequencies offer much more bandwidth than current cellular systems in the congested bands below 6 GHz, and initial capacity estimates have suggested that mmWave networks can offer orders of magnitude higher bit-rates than 4G systems [3].

However, the increased carrier frequency of mmWave systems makes the propagation conditions more demanding than at the lower frequencies traditionally used for wireless services, especially in terms of robustness. MmWave signals are blocked by many common building materials such as brick, and the human body can also significantly attenuate signals in the mmWave range [4]. Thus, the communication quality between the user equipment (UE) and any one cell can be highly variable as the movement of obstacles or even the changing position of the body relative to the mobile device can lead to rapid drops in signal strength. One likely key feature of mmWave cellular networks that can improve robustness is *multi-connectivity* (MC) [5], which enables each UE to maintain multiple possible signal paths to different cells so that drops in one link can be overcome by switching data paths. Multi-connectivity can be both among multiple 5G mmWave cells and between 5G mmWave cells and traditional 4G cells below 6 GHz. Mobiles with such 4G/5G multi-connectivity feature can benefit from both the high bit-rates that can be provided by the mmWave links, as well as the more robust, but lower-rate, legacy channels, thereby opening up new ways of solving capacity issues, as well as new ways of providing good mobile network performance and robustness [6].

This paper addresses one of the key challenges in supporting multi-connectivity in heterogeneous networks (HetNets) with mmWave cells, namely directional multi-cell channel tracking and measurement reports. These operations are fundamental for cellular systems to properly perform a wide variety of control tasks including handover, path selection, and radio-link failure (RLF) detection and recovery. However, while channel tracking and reporting is relatively straightforward in cellular systems at conventional frequencies, the mmWave bands present several significant limitations, including: (i) the high variability of the channel in each link due to blockage [7], [8]; (ii) the need to track multiple directions for each link [9]; and (iii) reports from the UE back to the cells must be made directional [10].

### A. Contributions

To address these challenges, in this paper we provide the first comprehensive numerical evaluation of the performance of a novel uplink (UL) multi-connectivity measurement reporting system which enables fast, robust and efficient cell selection. In such a scheme, the UE directionally broadcasts sounding reference signals (SRSs) in time-varying directions that continuously sweep the angular space. Each potential serving cell scans all its angular directions and monitors the strength of the received SRSs. A centralized controller (that can be identified by an LTE eNB operating in the legacy band) obtains complete directional knowledge from all the potential cells in the network to make the optimal serving cell selection and scheduling decision. We note that the proposed scheme should not be confused with a mmWave version of coordinated multipoint (CoMP) [11]. In CoMP, multiple eNBs simultaneously transmit to obtain beamforming gains across cells (in effect creating a high-dimensional antenna array). In the proposed method, although it measures control signals from multiple cells, the UE receives data from only one cell at a time. Importantly, unlike traditional CoMP, the eNB does not need to maintain relative phase information for the links from different cells - a task that would be extremely difficult in the mmWave setting due to the high Doppler. The proposed method is thus closer to carrier aggregation or fast handover.

As an extension of our work [1], in this paper we additionally aim at comparing the performance of the presented approach with respect to a traditional downlink-based standalone (SA) scheme. We numerically show that:

- The implementation of an UL-based framework enables a faster and less energy consuming tracking of the channel quality over time at the mobile terminal. In fact, an uplink sounding scheme eliminates the need for the UE to send measurement reports back to the network and thereby removes a possible point of failure in the control signaling path. Moreover, if digital beamforming or beamforming with multiple analog streams is available at the mmWave cell, then the directional scan time can be dramatically reduced when using UL-based measurements.
- The use of a MC approach enables a better performing resource allocation and mobility management with respect to a SA configuration. In fact, the LTE connectivity can offer a ready backup in case the mmWave links suffer an outage and can be used to forward the scheduling and serving decisions to the user if the main propagation path is unavailable.
- The presented framework guarantees robust and stable communication quality in the pres-

ence of the channel variations and dynamics expected at mmWaves.

Furthermore, we give numerical evidence of how the proposed UL-based framework enables the design of efficient 5G control plane applications and fundamental MAC layer functions that specify how a UE should connect to the network and preserve its connectivity. Specifically, our scheme allows for:

- Efficient and stable *handover*. Dense deployments of short range cells, as foreseen in future mmWave cellular networks, may exacerbate frequent handovers between adjacent eNBs [12]. High throughput values can be continuously guaranteed when intensively monitoring the UE's channel quality over time (even when considering highly dynamic environments).
- Fast and fair *initial access*. Unlike in traditional attachment policies, by leveraging on the presence of the local coordinator, the initial association can be possibly performed by taking into account the instantaneous load conditions of the surrounding cells, thereby promoting fairness in the whole cellular network.
- Reactive *RLF detection and recovery*. By exploiting previously saved instances of the channel quality information exchanged by the network nodes, a backup steering direction can be set in case the primary one is blocked, to immediately recover an acceptable communication service without waiting for a handover to be eventually triggered.

Finally, we evaluate the performance of the presented framework by considering a detailed real-world measurement-based mmWave channel scenario, for which we defined an innovative mobility model which accounts for the dynamics (in terms of both small and large scale fading) experienced by the mmWave links. Most of the studies so far have been conducted in stationary conditions with minimal local blockage, whereas this is one of the first contributions in which a dynamic environment is considered.

### B. Related Work

Channel estimation is relatively straightforward in LTE [13]. However, in addition to the rapid variations of the channel, transmissions in mmWaves are expected to be directional, and thus the network and the UE must constantly monitor the direction of transmission of each potential link. Tracking changing directions can slow the rate at which the network can adapt, and can be a major obstacle in providing robust service in the face of variable link quality. In addition, the UE and the eNB may only be able to listen to one direction at a time, thus making it hard to receive the control signaling necessary to switch paths.

Dual-connectivity has been proposed in Release 12 of Long Term Evolution-Advanced (LTE-A) [14]. This feature supports inter-frequency and intra-frequency connectivity as well as connectivity to different types of base stations (e.g., macro and pico base stations) [15]. However, these systems were designed for conventional frequencies, and did not address the directionality and variability of the channels present at mmWave frequencies.

Some other previous works, such as [16], consider the bands under 6 GHz as the only control channel for 5G networks, to provide robustness against blockage and wider coverage range. However, high capacities can also be obtained just exploiting the mmWave frequencies. So, in [5], a multi-connectivity framework is proposed as a solution for mobility-related link failures and throughput degradation of cell-edge users, relying on the fact that the transmissions from cooperating cells are coordinated for both data and control signals.

The work in [17] assumes a HetNet deployment of small cells and proposes that the control plane be handled centrally for small geographical areas whereas, for large geographical areas, distributed control should be used. However, the performance evaluation of small cells that use the same carrier frequency deployed over a relatively wider area has not yet been investigated.

Finally, in [18] we showed, through an extensive simulation campaign, that the proposed framework is suitable to enable fast network handover procedures. However, we did not investigate the performance of other interesting cellular control applications (i.e., initial access or RLF detection and recovery) and we did not account for the dynamics that affect the mmWave propagation.

## II. UPLINK MULTI-CONNECTIVITY PROCEDURE DESCRIPTION

In the presented framework, summarized in Tab. I, there is one major node called MCell (Master Cell, in accordance with 3GPP LTE terminology), which here is typically an LTE eNB operating in the legacy band. However, functionally, the MCell can be any network entity that performs centralized handover and scheduling decisions. The UE may receive data from a number of mmWave cells we refer to as SCells (Secondary Cells). In order to communicate and exchange control information, the S/MCells are interconnected via traditional backhaul X2 connections, while each user can be reached by its serving MCell through the legacy band.

MmWave SCells and UEs will likely utilize directional phase arrays for transmission. In this work, we assume that nodes select one of a finite number of directions, and we let  $N_{\text{SCell}}$  and  $N_{\text{UE}}$  be the number of directions at each SCell and UE, respectively. Thus, between any cell and the UE there are a total of  $N_{\text{SCell}} \times N_{\text{UE}}$  direction pairs. The key challenge in implementing

Tab. I: Description of the uplink-based multi-connectivity procedure presented in Sec. II

<p style="text-align: center;"><b>First Phase</b></p> <p style="text-align: center;">– UL Measurements –</p>	<ul style="list-style-type: none"> <li>• UE transmits the SRSs to the surrounding SCells, through directions <math>d_1, \dots, d_{N_{\text{UE}}}</math>.</li> <li>• SCell performs an exhaustive search to collect the SRSs, through directions <math>D_1, \dots, D_{N_{\text{SCell}}}</math>.</li> <li>• RTs are filled with the metrics <math>\text{SINR}_{i,j}, \forall i \in \{1, \dots, N\}, \forall j \in \{1, \dots, M\}</math>.</li> </ul>
<p style="text-align: center;"><b>Second Phase</b></p> <p style="text-align: center;">– Coordination –</p>	<ul style="list-style-type: none"> <li>• SCell sends its RT to the MCell, through the backhaul link.</li> <li>• MCell builds a CRT by collecting all the received RT.</li> <li>• MCell makes attachment decisions by selecting the optimal SCell for each UE to connect to.</li> </ul>
<p style="text-align: center;"><b>Third Phase</b></p> <p style="text-align: center;">– Decision –</p>	<ul style="list-style-type: none"> <li>• MCell forwards the best decision for the transceiver.</li> <li>• SCell is informed through the backhaul link.</li> <li>• UE is informed through the LTE legacy band, to remove a point of failure in the feedback.</li> </ul>

multi-cell connectivity is that the network must monitor the signal strength on each of the direction pairs for each of the possible links. This is done by each SCell building a *report table* (RT) for each user, based on the channel quality of each receiving direction that can be used by the central entity to: (i) help the UE identify the mmWave eNB with the best instantaneous propagation conditions, and (ii) trace and estimate, over time, the channel quality conditions.

The system can be more precisely described as follows. Suppose that, in the considered area,  $M$  SCells and  $N$  UEs are deployed under the control of one MCell. The framework performs its monitoring operations through three main phases.

#### A. First phase: Uplink measurements

In the MC procedure's first phase, each SCell fills its RT. Each UE directionally broadcasts uplink sounding reference signals in dedicated slots, steering through directions  $d_1, \dots, d_{N_{\text{UE}}}$ , one at a time, to cover the whole angular space. The SRSs are scrambled by locally unique identifiers (e.g., C-RNTI) that are known to the SCells. We are therefore exploiting an UL measurement reporting system where, unlike in traditional mechanisms, the reference signals are broadcast by each UE rather than by the eNBs. The advantages of this design choice will be explained in the next sections of this work. If analog beamforming is used, each SCell performs an exhaustive search, scanning through directions  $D_1, \dots, D_{N_{\text{SCell}}}$ , one at a time or, if digital beamforming is

applied, from all of them at once<sup>1</sup>.

Each SCell fills its RT whose entries represent the highest Signal-to-Interference-plus-Noise-Ratio (SINR) between UE<sub>*i*</sub>,  $i \in \{1, \dots, N\}$ , transmitting through its best direction  $d_{\text{UE,opt}} \in \{d_1, \dots, d_{N_{\text{UE}}}\}$  and the SCell<sub>*j*</sub>,  $j \in \{1, \dots, M\}$ , receiving through its best possible direction  $D_{\text{SCell,opt}} \in \{D_1, \dots, D_{N_{\text{SCell}}}\}$ :

$$\text{SINR}_{i,j}(d_{\text{UE,opt}}, D_{\text{SCell,opt}}) = \underset{\substack{d_{\text{UE}}=d_1, \dots, d_{N_{\text{UE}}} \\ D_{\text{SCell}}=D_1, \dots, D_{N_{\text{SCell}}}}}{\arg \max} \text{SINR}_{i,j}(d_{\text{UE}}, D_{\text{SCell}}) \quad (1)$$

### B. Second Phase: Coordination

Once the RT of each SCell has been filled, each mmWave cell sends this information, through the backhaul link, to the supervising MCell which, in turn, builds a *complete report table (CRT)*, as depicted in Tab. II. The controller has indeed a complete overview of the surrounding channel conditions and gains a comprehensive vision over the whole cellular system it oversees. When accessing the CRT, the MCell eventually makes a network decision by selecting the best candidate mmWave SCell for each user to connect to, based on different metrics (i.e., the maximum SINR, with some hysteresis, or the maximum rate, when being aware of the current load of each cell).

For example, if the maximum SINR attachment policy is selected, the UE<sub>*i*</sub>,  $i \in \{1, \dots, N\}$  will be associated with the mmWave SCell<sub>*j*</sub>,  $j \in \{1, \dots, M\}$ , if the entry

$$\text{SINR}_{i,j}(d_{\text{UE,opt}}, D_{\text{SCell,opt}})$$

is the highest one in the *i*-th row of the CRT. Such maximum SINR is associated, in the CRT's entry, to the SCell (UE) optimal direction  $D_{\text{SCell,opt}}(d_{\text{UE,opt}})$ , which should therefore be selected to reach the UE (SCell) with the best performance.

### C. Third Phase: Network Decision

If the serving cell needs to be switched, or a secondary cell needs to be added or dropped, the MCell needs to inform both the UE and the mmWave eNB. Since the UE may not be listening in the direction of the target SCell, the UE may not be able to hear a command from that cell. Moreover, since path switches and cell additions in the mmWave regime are commonly

<sup>1</sup>The synchronization between the sweeping of the users and the listening of the base stations in the mmWave band is guaranteed by assuming that the mobile terminals have already exchanged some preliminary time/frequency synchronization information through the LTE connectivity.

Tab. II: An example of CRT, referred to  $N$  users and  $M$  available mmWave SCells in the network. We suppose that the UE can send the sounding signals through  $N_{\text{UE}}$  angular directions and each mmWave eNB can receive them through  $N_{\text{SCell}}$  angular directions. Each pair is the maximum SINR measured in the best direction between the UE ( $d_{\text{UE,opt}}$ ) and the SCell ( $D_{\text{SCell,opt}}$ ).

Complete Report Table (CRT)			
UE	mmWave SCell <sub>1</sub>	...	mmWave SCell <sub>M</sub>
UE <sub>1</sub>	SINR <sub>1,1</sub> ( $d_{\text{UE,opt}}$ , $D_{\text{SCell,opt}}$ )	...	SINR <sub>1,M</sub> ( $d_{\text{UE,opt}}$ , $D_{\text{SCell,opt}}$ )
UE <sub>2</sub>	SINR <sub>2,1</sub> ( $d_{\text{UE,opt}}$ , $D_{\text{SCell,opt}}$ )	...	SINR <sub>2,M</sub> ( $d_{\text{UE,opt}}$ , $D_{\text{SCell,opt}}$ )
...	...	...	...
UE <sub>N</sub>	SINR <sub>N,1</sub> ( $d_{\text{UE,opt}}$ , $D_{\text{SCell,opt}}$ )	...	SINR <sub>N,M</sub> ( $d_{\text{UE,opt}}$ , $D_{\text{SCell,opt}}$ )

due to link failures, the control link to the serving mmWave cell may not be available either. To handle these circumstances, we propose that the path switch and scheduling commands be communicated over the coordinator operating in the legacy band.

Therefore, the MCell notifies the designated optimal mmWave SCell, via the high capacity backhaul, about the UE's desire to attach to it. It also embeds the best direction  $D_{\text{SCell,opt}}$  that should be set to reach that user. Moreover, supposing that the UE has already set up a link to the LTE eNB, on a legacy connection, the MCell sends to the UE, through an omnidirectional control signal at sub-6 GHz frequencies, the best user direction  $d_{\text{UE,opt}}$  to select, to reach such candidate SCell. By this time, the best SCell-UE beam pair has been determined, therefore the transceiver can directionally communicate in the mmWave band.

We recall that the attachment decision is performed neither by the user nor by the designated mmWave SCells, but rather by the supervising MCell, which is the only entity having a clear and complete overview of the channel propagation conditions. This guarantees much higher reliability (since the low frequencies at which the coordinator operates can easily penetrate through obstacles) and fairness (since the attachment decision is periodically triggered by taking into consideration the propagation conditions of the whole cellular network) in the communication system.

### III. ENABLING 5G CONTROL APPLICATIONS

Existing MAC and lower-layer control procedures already implemented in a variety of traditional wireless systems should be revised and adapted to the unique mmWave radio environment in which next-generation networks are expected to operate.



**Cellular.** Next-generation cellular systems must provide a mechanism by which UEs and mmWave eNBs establish highly directional transmission links, typically formed with high-dimensional phased arrays, to benefit from the resulting beamforming gain and balance for the increased isotropic pathloss experienced at high frequencies. In this context, directional links require fine alignment of the transmitter and receiver beams, an operation which might dramatically increase the time it takes to access the network [10]. Moreover, the dynamics of the mmWave channel imply that the directional path to any cell can deteriorate rapidly, necessitating an intensive tracking of the mobile terminal.

**Vehicular.** Advanced and sophisticated sensors future cars will be equipped with will require an unprecedented amount of data to be exchanged, which goes beyond the capabilities of existing technologies. On the one hand, the mmWave frequencies have the potential to support the required higher data rates. On the other hand, there are many concerns regarding the transmission characteristics of the mmWave channels in an automotive environment [19]. For instance, once the nodes are directionally connected, the alignment can be maintained by using beam tracking mechanisms that try to maintain a consistent view of the most favorable beam directions over time. However, in highly dense or highly mobile vehicular scenarios, the corresponding peer may change frequently and may not last long enough to allow the completion of a data exchange, thus resulting in transmission errors. Moreover, the increased Doppler effect could make the assumption of channel reciprocity not valid and could impair the feedback over mmWave links, which is a potential point of failure for beam sweeping. Re-alignment of the beams is therefore required to maintain connectivity.

**802.11ad.** The IEEE 802.11ad standard operates in the 60 GHz millimeter wave spectrum and therefore currently designed control protocols already address some of the requirements and challenges pertaining to a high-frequency environment. However, most proposed solutions are unsuitable for future 5G mmWave mobile network requirements, since they present many limitations (e.g., they are appropriate for short-range, static, and indoor scenarios, which do not match well the requirements of 5G systems). Therefore, new specifically designed solutions for dynamic networks need to be found.

As we will numerically show in Sec. V and discuss in Sec. III-A – III-C, we claim that faster, more efficient and more robust control plane applications (including handover, beam tracking, initial access, RLF recovery) can be enabled when considering a multi-connectivity system, with respect to the case in which a standalone scheme is preferred.

### A. Handover and Beam Tracking

Handover is performed when the UE moves from the coverage of one cell to the coverage of another cell [20]. Beam tracking refers to the need for a user to periodically adapt its steering direction, to realign with its serving eNB, if it has moved or the channel propagation conditions have changed over time. Frequent handover, even for fixed UEs, is a potential drawback of mmWave systems due to their vulnerability to random obstacles, which is not the case in LTE. Dense deployments of short range eNBs, as foreseen in mmWave networks, may exacerbate frequent handovers between adjacent eNBs. Loss of beamforming information due to channel change is another reason for handover and reassociation [12].

The literature on handover and beam tracking in more traditional sub-6 GHz heterogeneous networks is quite mature. For instance, the survey in [21] and the work in [22] present multiple vertical handover decision algorithms that are essential for wireless networks while, in [13], omnidirectional pilots are used for channel estimation. However, most works are specifically tailored to low-frequency legacy cellular systems, whose features are largely different from those of a mmWave environment, preventing the proposed techniques from being applicable to next-generation 5G scenarios. On the other hand, papers on mobility management for mmWave networks (e.g., [18], [23]–[26]) are very recent, since research in this field is just at its infancy.

We argue that, when considering a higher frequency setting, the presented MC framework can ensure more efficient mobility management operations by exploiting the centralized MCell control over the network to: (i) periodically determine the UE’s optimal mmWave SCell to associate with (if handover is strictly required<sup>2</sup>), or (ii) the new direction through which it should steer the beam (if a simple beam adaptation event guarantees a sufficiently good communication quality), when the user is in *connected-mode*, i.e., it is already synchronized with both the LTE and the mmWave cells. The key input information for the handover/beam tracking decision includes (i) instantaneous channel quality, (ii) channel robustness, and (iii) cell occupancy.

With respect to the existing algorithms, the use of both the sub-6 GHz and the mmWave control planes is a key functionality for such a technique. In fact, especially when considering highly unstable and scarcely dense scenarios, the LTE connectivity ensures a ready backup in case the

<sup>2</sup>In order to reduce the handover frequency, more sophisticated decision criteria could be investigated, rather than triggering a handover every time a more suitable SCell is identified (i.e., the reassociation might be performed only if the SINR increases above a predefined threshold, with respect to the previous time instant). A more detailed discussion of the different handover paradigms is beyond the scope of this paper and we refer the interested reader to [18] for further details.

mmWave links suffer an outage. Furthermore, the handover/beam switch decision is forwarded to the UE through the MCell, whose legacy link is much more robust and less volatile than its mmWave counterpart, thereby removing a possible point of failure in the control signaling path. Since each SCell periodically forwards the RT, the MCell has a complete overview of the cell dynamics and propagation conditions and can accordingly make network decisions, to maximize the overall performance of the cell it oversees, as we will numerically show in Sec. V-B. Moreover, unlike in the traditional procedures in which the users are not aware of the surrounding cells' current state, the UE may choose to connect to the SCell providing either the maximum SINR or the maximum rate (depending on what is considered more convenient), thus taking into account the load of each mmWave cell.

We finally remark that, if previous versions of the report table are kept as a record, the MCell can also use the SCells' quality variance in selecting the mmWave eNB a user should attach to, after a handover is triggered. If a selected SCell shows a large variance (which reflects high channel instability), the user might need to handover again in the very near future. Therefore, it could be better to trigger a handover only to an SCell which grants both good SINR (or rate) and sufficient channel stability, leading to a more continuous and longer-term network association. We will address this analysis as part of our future work.

### *B. Initial Access*

The procedure described in the previous subsection is referred to a UE that is already connected to the network. However, we show that an uplink-based multi-connectivity control approach may allow for fast initial access (IA) from idle mode too. Initial access [10], [27] is the procedure by which a mobile UE establishes an initial physical link connection with a cell, a necessary step to access the network. In current LTE systems, IA is performed on omnidirectional channels [20]. However, in mmWave cellular systems, transmissions will need to be directional to overcome the increased isotropic pathloss experienced at higher frequencies. IA must thus provide a mechanism by which the eNB and the UE can determine suitable initial directions of transmission.

MmWave initial access procedures have been recently analyzed in [8], [28]–[30]. Different design options have been compared in [10], [27], to evaluate coverage and access delay. We refer to [10] for a more detailed survey of recent IA works. All of these methods are based on the current LTE design in which each cell broadcasts synchronization signals and each UE scans the directional space to find the optimal node to potentially connect to. A key result of these

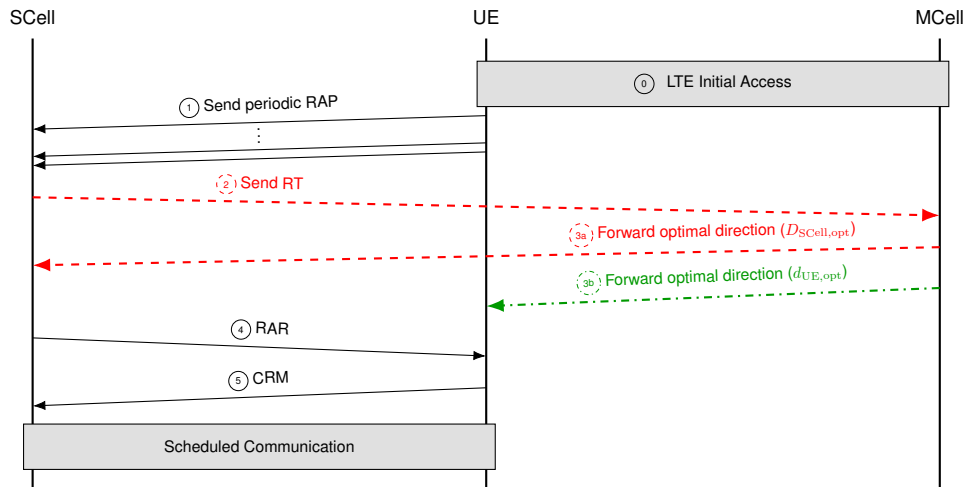


Fig. 1: Proposed uplink multi-connectivity initial access procedure. Red and green dashed lines refer to the control messages exchanged via the bachaul X2 and the legacy communication links, respectively.

schemes is that the dominant delay in downlink-based IA arises in this initial synchronization phase. We therefore propose an alternate uplink scheme, as shown in Fig. 1, primarily based on the MC framework described in Sec. II. According to the LTE terminology:

- 0) A user searches for synchronization signals from conventional 4G cells. This detection is fast since it can be performed omnidirectionally and there is no need for directional scanning<sup>3</sup>.
- 1) A user desiring initial access broadcasts a *random access preamble* (RAP) scanning different angular directions, while the mmWave cells scan for the presence of those messages. According to the MC procedure's first phase, multiple RTs are collected at the SCell sides. Each of these RAPs will arrive roughly time-aligned in the random access slots of all potential neighboring mmWave cells.
- 2) Each SCell forwards its RT to the MCell via the X2 backhaul link. In analogy with the MC's second phase, the MCell performs the best attachment decision, based on the received RTs, together with selecting the optimal directions for the transceiver to communicate.
- 3) The MCell forwards to the designated SCell (via the usual high capacity backhaul) and to the user (via the legacy LTE band though an omnidirectional control message) the respective sectors through which they should steer the beam to communicate.

<sup>3</sup> Under the assumption that the 5G mmWave eNBs are roughly time synchronized to the 4G cell, and the round trip propagation times are not large, an uplink transmission from the UE will be roughly time aligned at any closeby mmWave cell. For example, if the cell radius is 150 m (a typical mmWave cell), the round trip delay is only 3  $\mu$ s.

- 4) At this point, the best SCell-UE beam pair has been determined, therefore both the user and the SCell can steer through their optimal directional sectors, obtaining the full beamforming gain. So, the SCell transmits a *random access response* (RAR) to the UE, containing some initial timing and power correction information.
- 5) After receiving the RAR, the UE sends a *connection request message* (CRM) on the resources scheduled in the grant in the RAR. All subsequent communication can occur on scheduled channels. As in 3GPP LTE, the immediate subsequent messages would be used for connection set up and contention resolution [28].

The performance of the presented IA procedure will be analyzed in detail in Sec. V-C. Anyway, we immediately notice that the attachment decision is made by the MCell, which oversees the whole network and collects channel reports from all the surrounding mmWave cells. Therefore, unlike in traditional attachment policies, the association can be possibly performed by accounting for the instantaneous load conditions of the neighboring cells, to guarantee enough fairness and reliability to the whole cellular network. Furthermore, we claim that an uplink-based scheme allows for faster IA than its downlink counterpart, especially when a beamforming architecture with multiple analog streams is preferred for the sweeping operations.

### C. RLF Detection and Recovery

One of the key challenges systems operating in mmWave bands have to cope with is the rapid channel dynamics. Unlike in conventional LTE systems, mmWave signals are completely blocked by many common building materials such as brick and mortar. As a result, the movement of obstacles and reflectors, or even changes in the orientation of a handset relative to a body or hand, can cause the channel to rapidly appear or disappear [31]. When a radio-link failure (RLF) occurs, the link that has been established between user and eNB is obstructed, with a consequent SINR and throughput degradation. The UE should immediately react by adapting its beam pair or, as a last resort, by triggering a handover [9].

Most literature refers to challenges that have been recently analyzed in the 60 GHz IEEE 802.11ad WLAN and WPAN scenarios. In [32], for example, a detailed investigation of the effect of people movement on the temporal fading envelope is performed. Some related works present different solutions to address the blockage issue described above, such as [33]–[35].

In the event that the primary propagation path is obstructed, the MC procedure presented in Sec. II can be employed to partially overcome the link failure leveraging on: (i) the presence of

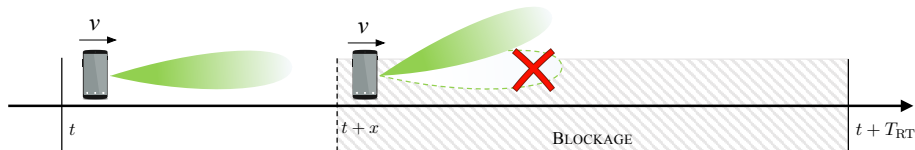


Fig. 2: MC procedure for RLF recovery. At time  $t$  and  $t + T_{RT}$  the SCell collects a RT. At time  $t + x$  a blockage event occurs and the user, moving at constant velocity  $v$ , loses the connection with its current serving mmWave SCell. The UE and the SCell can promptly react to the channel failure by exploiting previously saved report table entries.

the central controller and the very reliable and stable LTE connection the UEs can benefit from, and (ii) previously saved instances of the channel quality information exchanged by the network nodes. We use Fig. 2 as an example. Assume that, at time  $t$ , the user moving at constant speed  $v$  is connected to a specific mmWave SCell, through direction  $d_{UE,opt}$ . We assume that, at time  $t+x$  and before a new RT is generated, a blockage occurs. If no practical actions are taken, the user has to wait for a new RT to be collected (at time  $t + T_{RT}$ ) before a new optimal beam pair, able to circumvent the obstruction, is determined. Indeed, during  $T_{RT} - x$  s, the user's experienced rate is zero, due to the link breakdown and the consequent SINR collapse. One practical solution is to immediately react to the path impairment by taking advantage of previously saved instances of the RT. As soon as a blockage is detected, the UE can autonomously access its most recent RT entries (or set of previous tables) and find the second best direction  $d_{UE,subopt} \neq d_{UE,opt}$  to communicate, as a sort of *backup procedure* before the transceiver fully recovers the optimal beam configuration. Such beam pair will be a suboptimal solution (since the optimal path is blocked), but at least allows the user to experience a higher average throughput than it would have achieved if no actions were taken.

Having a second available link, when the primary path is obstructed, adds diversity and robustness to the communication. In Sec. V-D, we will numerically show the advantages, in terms of throughput, of establishing a backup beam configuration between UE and eNB, after a RLF is detected, rather than just waiting for a complete network decision to be made.

#### IV. SIMULATION PARAMETERS DESCRIPTION

In Sec. IV-A, we describe the mmWave and the LTE channel models we used to run the simulations, and in Sec. IV-B we present the mobility model we employed to account for the dynamics which affect the mmWave propagation. Finally, in Sec. IV-C, we present our main simulation parameters.

### A. Channel Models

**Mmwave Channel Model.** The channel model we have implemented is based on recent real-world measurements at 28 GHz in New York City, to provide a realistic assessment of mmWave micro and picocellular networks in a dense urban deployment. The parameters that are used to generate one instance of the channel matrix  $\mathbf{H}$  include: (i) spatial clusters; (ii) fractions of power; (iii) angular beamspreads; and (iv) a small-scale fading model, massively affected by the Doppler shift, where each of the path clusters is synthesized with a large number of subpaths. A complete description of the channel parameters can be found in [3], [36], [37].

The distance-based pathloss, which models Line-of-Sight (LoS), Non-Line-of-Sight (NLoS) and outage, is defined as  $PL(d)[dB] = \alpha + \beta 10 \log_{10}(d)$ , where  $d$  is the distance between the receiver and the transmitter and the values of the parameters  $\alpha$  and  $\beta$  are given in [3].

Due to the high pathloss experienced at mmWaves, multiple antenna elements with beamforming (BF) are essential to provide an acceptable communication range. The BF gain from transmitter  $i$  to receiver  $j$  is given by:

$$G_{\text{BF}}(i, j) = |\mathbf{w}_{rx,ij}^* \mathbf{H}_{ij} \mathbf{w}_{tx,ij}|^2 \quad (2)$$

where  $\mathbf{H}_{i,j}$  is the channel matrix of the  $ij^{\text{th}}$  link,  $\mathbf{w}_{tx,ij} \in \mathbb{C}^{n_{\text{Tx}}}$  is the BF vector of transmitter  $i$  when transmitting to receiver  $j$ , and  $\mathbf{w}_{rx,ij} \in \mathbb{C}^{n_{\text{Rx}}}$  is the BF vector of receiver  $j$  when receiving from transmitter  $i$ . Analog or digital beamforming architectures are typically considered. The former shapes the output beam with only one radio frequency (RF) chain, using phase shifters. This model saves power by using only a single Analog-to-Digital Converter (ADC) but has limited flexibility since the eNBs can only beamform in one direction at a time. On the other hand, the latter configuration provides the highest flexibility in shaping the beams, allowing transmission/reception in multiple directions simultaneously. However, it requires one RF chain per antenna element, thus increasing the cost and complexity of the architecture [38].

The channel quality is measured in terms of SINR. By referring to the mmWave statistical channel described above, the SINR between eNB $_m$  and a test UE is:

$$\text{SINR}(m) = \frac{\frac{P_{\text{TX}_{\text{mmW}}}}{PL_m} G_{\text{BF}}(m, \text{UE})}{\sum_{k \neq m} \frac{P_{\text{TX}_{\text{mmW}}}}{PL_k} G(k, \text{UE}) + W_{\text{mmW}} \times N_0} \quad (3)$$

where  $G_{\text{BF}}(m, \text{UE})$  and  $PL_m$  are the BF gain and the pathloss obtained between eNB $_m$  and the UE, respectively, and  $W_{\text{mmW}} \times N_0$  is the thermal noise. In (3), it is assumed that the UE is

interfered by other transmitters. However, to some extent, given the wide bandwidth, it is easy to orthogonalize the SRSs across multiple users and we can assume that the SRS waveforms are transmitted over multiple sub-signals with each sub-signal being transmitted over a small bandwidth  $W_{\text{sig}}$ . The use of the sub-signals can provide frequency diversity, and narrowband signals in the control plane remove any inter-cell interference and support low power receivers with high SINR capabilities [28].

Finally, the rate ( $R$ ) experienced by the UE connected to eNB $_m$  is approximated using the Shannon capacity:

$$R(m) = \frac{W_{\text{mmW}}}{N_m} \log_2 \left( 1 + \text{SINR}(m) \right) \quad (4)$$

where  $N_m$  is the number of users that are currently being served by eNB $_m$  and  $W_{\text{mmW}}$  is the available total bandwidth.

**LTE Channel.** A connection to the LTE band is required when the mmWave primary propagation path is obstructed or not available, or to reliably forward the scheduling/attachment decisions to the final user. According to the LTE 3GPP specifications in [14] and considering an outdoor dense scenario, a distance-dependend pathloss from the MCell to the UE can be defined. In particular, assuming that the user, being at distance  $R$  from the LTE eNB, is in a LoS pathloss state, with probability

$$\mathbb{P}_{\text{LoS}}(R) = \min \left( \frac{0.018}{R}, 1 \right) \left[ 1 - \exp \left( \frac{-R}{0.063} \right) \right] + \exp \left( \frac{-R}{0.063} \right), \quad (5)$$

the LoS pathloss can be defined as:

$$PL_{\text{LoS}}(R) = 103.4 + 24.2 \log_{10}(R). \quad (6)$$

Conversely, if a NLoS condition holds (with probability  $\mathbb{P}_{\text{NLoS}}(R) = 1 - \mathbb{P}_{\text{LoS}}(R)$ ), the NLoS pathloss can be defined as:

$$PL_{\text{NLoS}}(R) = 131.1 + 42.8 \log_{10}(R). \quad (7)$$

When considering an LTE connection, signals are assumed to be exchanged through omnidirectional channels. Therefore, if we deploy just one LTE eNB in the reference scenario, the quality of the received information is measured, in terms of SNR, by:

$$\text{SNR} = \frac{P_{\text{TXLTE}}/PL(R)}{W_{\text{LTE}} \times N_0}, \quad (8)$$

where  $PL(R)$  is the pathloss (either LoS or NLoS) experienced between the MCell and the test UE, and  $W_{\text{LTE}} \times N_0$  is the thermal noise. The rate can be computed according to Eq. (4).



## B. Mobility Model

One of the key challenges for cellular systems in the mmWave bands is the rapid channel dynamics. When moving, the user experiences a strong Doppler shift whose effect increases with speed. However, most channel studies have been performed in stationary locations with minimal local blockage, making it difficult to estimate the fluctuations that affect a realistic mmWave environment. In order to simulate such dynamics, we propose a mobility model in which the small and the large scale fading parameters of the mmWave  $\mathbf{H}$  matrix are periodically updated, to emulate short variations and sudden changes of the perceived channel, respectively.

The Doppler shift and the spatial signatures are updated at every time slot, according to the user speed and its position, in terms of angle of arrival (AoA) and departure (AoD). The distance-based pathloss is also updated, but we maintain the same pathloss state (LoS, NLoS or outage) recorded in the previous complete update of the  $\mathbf{H}$  matrix. On the other hand, to capture the effects of the long term fading, the  $\mathbf{H}$  matrix parameters (i.e., the number of spatial clusters and subpaths, the fractions of power, the angular beamspreads and the pathloss conditions) are completely updated every  $T_H$  s, for all the mmWave links between each UE and each SCell. We recall that this may cause the user to switch from a certain pathloss state to another (e.g., from LoS to NLoS, to simulate the presence of an obstacle between transmitter and receiver), with a consequent sudden drop of the channel quality by many dBs.

The beamforming vectors are not adapted when the  $\mathbf{H}$  matrix is updated. We need to wait for a new RT to be collected (every  $T_{RT}$  s) to detect the (possibly changed) channel propagation conditions and properly react, i.e., by adapting the directions through which the UE and the designated SCell steer their beams. Frequent RTs (small  $T_{RT}$ ) and flat channels (large  $T_H$ ) result in a good monitoring of the user and good average channel gains. In Sec. V-B we show how variations of  $T_{RT}$  and  $T_H$  affect the communication quality.

As an example, in Fig. 3 we plot the rate experienced by a test user, moving at speed  $v = 20$  m/s along a straight line during an excerpt of a simulation. The large scale fading parameter of the mmWave channel are updated every  $T_H = 200$  ms, while the communication configuration may be updated every  $T_{RT} = 1$  s, upon the dissemination of the RTs to the MCell. For instance, it can be seen that, at time  $t = 2^-$ , the rate has strongly degraded, since the user has moved without updating its beam steering direction and thus has misaligned from its serving SCell. However, at time  $t = 2$ , a new CRT has been generated and the transceiver is finally able to update its beam configuration (by performing a beam switch operation) or the user can

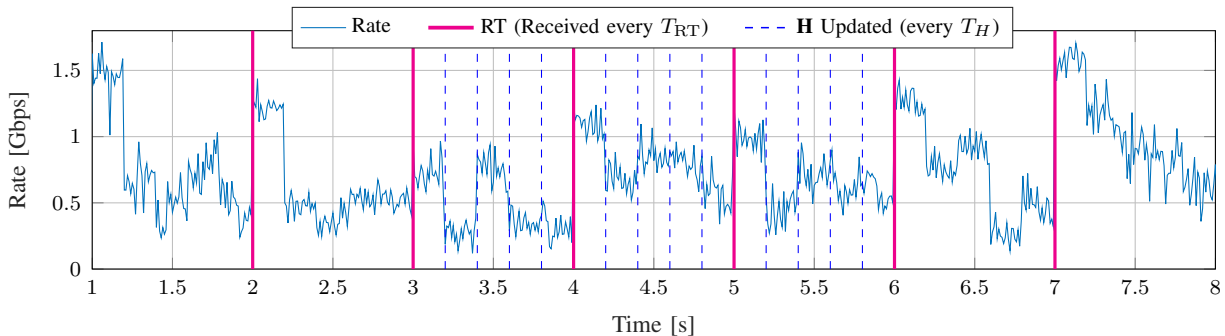


Fig. 3: Example of time-varying rate experienced by a user moving at speed  $v = 20$  m/s in a mmWave scenario in which  $M = 70$  BS/km<sup>2</sup> are deployed. The RTs are generated every  $T_{RT} = 1$  s (vertical magenta lines), the small scale fading parameters of the channel vary every time slot of 1 ms, the large scale fading parameters of the channel matrix  $\mathbf{H}$  vary every  $T_H = 200$  ms (vertical blue dotted lines).

handover (by choosing a serving mmWave eNB providing better communication performance), thus recovering the maximum achievable transmission rate. We notice that wide rate collapses (e.g., at time  $t = 3.2$  or  $t = 5.2$ ) mainly refer to pathloss state changes (i.e., from LoS to NLoS), caused by the update of the large scale fading parameters of  $\mathbf{H}$ , while the rapid fluctuations of the rate are due to the adaptation of the small scale fading parameters of the channel (and mainly to the Doppler effect experienced by the moving user).

### C. Simulation Scenario

The parameters used to run our simulations are based on realistic system design considerations and are summarized in Tab. III. Our results are derived through a Monte Carlo approach, where multiple independent simulations of duration  $T_{sim}$  are repeated, to get different statistical quantities of interest. In each experiment: (i) under the control of one single MCell operating in the legacy band, we deploy  $M$  mmWave SCells and  $N$  UEs, according to a Poisson Point Process (PPP) and as done in [39], with an average density of  $N_m = 10$  users per cell (as foreseen in [40] for a dense urban environment); (ii) we run the multi-connectivity framework described in Sec. II by establishing a mmWave link between each SCell-UE pair and collecting the SINR values at each SCell, according to Eq. (3), when the transceiver performs the sequential scan; and (iii) we select the most profitable mmWave eNB the user should attach to, according to either a maximum SINR or maximum rate policy.

We consider an SINR threshold  $\Gamma_{out} = -5$  dB, assuming that, if  $SINR_{i,j}(m) < \Gamma_{out}$ , no control signals are collected when the UE transmits through direction  $i$  and the BS  $m$  is receiving

Tab. III: Main simulation parameters.

Parameter	Value	Description
$W_{\text{mmW}}$	1 GHz	Bandwidth of mmWave eNBs
$f_{\text{c,mmW}}$	28 GHz	mmWave carrier frequency
$P_{\text{TX,mmW}}$	30 dBm	Transmission power of mmWave eNBs
$W_{\text{LTE}}$	20 MHz	Bandwidth of LTE eNB
$f_{\text{c,LTE}}$	2 GHz	LTE carrier frequency
$P_{\text{TX,LTE}}$	46 dBm	Transmission power of LTE eNB
$\Gamma_{\text{out}}$	-5 dB	Minimum SINR threshold
$N_{\text{ANT,SCell}}$	$8 \times 8$	SCell UPA MIMO array size
$N_{\text{ANT,UE}}$	$4 \times 4$	UE UPA MIMO array size
$N_{\text{SCell}}$	16	SCell scanning directions
$N_{\text{UE}}$	8	UE scanning directions
$T_{\text{sim}}$	10 s	Simulation duration
$v$	20 m/s	UE speed
$M$	Varied	mmWave SCell density
$N_m$	10	Users per mmWave SCell
$T_{\text{sig}}$	$10 \mu\text{s}$	SRS duration
$\phi_{\text{ov}}$	5%	Overhead
$T_{\text{per}}$	$200 \mu\text{s}$	Period between PSS transmissions
$T_H$	Varied	Channel update periodicity
$T_{\text{RT}}$	Varied	Time between two consecutive RTs
$T_B$	Varied	Blockage duration

through direction  $j$ . Decreasing  $\Gamma_{\text{out}}$  would allow finding more SCells, at the cost of designing more complex (and expensive) receiving schemes, able to detect the intended signal in more noisy channels. If a multi-connectivity approach is chosen, the UE can still reach the MCell (by establishing a connection over the LTE band) when the signal quality is below  $\Gamma_{\text{out}}$ .

A set of two dimensional antenna arrays is used at both the mmWave eNBs and the UE. SCells are equipped with a Uniform Planar Array (UPA) of  $8 \times 8$  elements, which allow them to steer beams in  $N_{\text{SCell}} = 16$  directions; the user exploits an array of  $4 \times 4$  antennas, steering beams through  $N_{\text{UE}} = 8$  angular directions<sup>4</sup>. The spacing of the elements is set to  $\lambda/2$ , where  $\lambda$  is the wavelength.

In the first phase of the presented sweeping algorithm, we alternate portions of time in which SRSs are periodically transmitted in brief intervals of length  $T_{\text{sig}}$ , and intervals of length  $T_{\text{per}} \gg T_{\text{sig}}$  in which each eNB and each UE handle their usual traffic operations. We took  $T_{\text{sig}} = 10 \mu\text{s}$ , which is sufficiently small that the channel will be coherent even at the very high frequencies for mmWaves, and  $T_{\text{per}} = 200 \mu\text{s}$ , in order to maintain a constant overhead of

<sup>4</sup>In this work, we assume a 2D structure for the cells. Nevertheless, our system is easily customizable and allows for the design of an advanced 3D scanning technique as well. However, such a choice would lead to an increase of the time required to complete each iteration of the presented measurement reporting scheme, without providing any further noticeable insights.

$\phi_{\text{ov}} = 5\%$ . In this way, the mmWave eNBs will be taken out of their standard communication capabilities only for  $\phi_{\text{ov}} = T_{\text{per}}/T_{\text{sig}} = 5$  percent of their operational time<sup>5</sup>.

## V. RESULTS AND PERFORMANCE EVALUATION

In this section, we present some simulation results aiming at:

- (i) comparing the performance of the uplink multi-connectivity framework described in Sec. II with a traditional downlink standalone approach in terms of delay, data rate, energy consumption and stability;
- (ii) giving numerical evidence of the performance of several control applications (i.e., handover, beam tracking, initial access, RLF recovery) which can be enabled in next-generation mmWave systems by the presented measurement reporting framework;
- (iii) showing how the variability of the mmWave channel affects the performance of a cellular network (mainly in terms of achievable throughput).

### A. Comparison with Downlink Standalone Scheme

**Delay.** We define as  $D$  the time *delay* required to complete each iteration of either the uplink multi-connectivity framework presented in this work or a traditional downlink standalone scheme. We claim that the first phase of the proposed framework (i.e., uplink measurements) dominates the overall delay performance, provided that: (i) the switching time for beam switching is in the scale of nanoseconds, and so it can be neglected [41]; (ii) in the second phase of the procedure, according to [18], RTs are sent through the X2 links, which may be wired or wireless backhaul and whose latency is assumed to be negligible. In addition, the backhaul overhead is minimal since it requires only transmission of Channel Quality Indicator (CQI) levels for each cell, which is very small compared to the data; (iii) in the third phase of the procedure, the attachment decisions are once again forwarded to the SCells through the high capacity backhaul and through omnidirectional LTE messages, whose latency is ignored if the UEs have already set up a link to the MCell.

Following [8], [28], we suppose that in either the uplink or the downlink direction, the synchronization signals are  $T_{\text{sig}}$  long and occur once ever  $T_{\text{per}}$  s. The size of  $T_{\text{sig}}$  is determined by the necessary link budget and we will assume that it is the same in both directions. The

<sup>5</sup>The values of  $T_{\text{per}}$  and  $T_{\text{sig}}$  have been chosen according to the analysis in [10], [27], [28]. However, the proposed framework is general and its parameters can be tuned according to the peculiarities of any specific simulation environment.

Tab. IV: Delay  $D$  to complete each iteration of either the uplink multi-connectivity measurement framework described in Sec. II or a traditional downlink standalone approach. A comparison among different BF architectures (analog and fully digital) is performed. We assume  $T_{\text{sig}} = 10 \mu\text{s}$ ,  $T_{\text{per}} = 200 \mu\text{s}$  (to maintain an overhead  $\phi_{\text{ov}} = 5\%$ ),  $N_{\text{SCell}} = 16$  and  $N_{\text{UE}} = 8$ .

BF Architecture	UL Scheme UEs transmit SCells receive	DL Scheme UEs receive SCells transmit
Analog	$N_{\text{SCell}}N_{\text{UE}}T_{\text{per}}$ (25.6 ms)	$N_{\text{SCell}}N_{\text{UE}}T_{\text{per}}$ (25.6 ms)
Digital <sup>(*)</sup>	$\frac{N_{\text{SCell}}N_{\text{UE}}T_{\text{per}}}{N_{\text{SCell}}}$ (1.6 ms)	$\frac{N_{\text{SCell}}N_{\text{UE}}T_{\text{per}}}{N_{\text{UE}}}$ (3.2 ms)

<sup>(\*)</sup> Digital beamforming is applied at the receiver (i.e., at the SCell side if an UL scheme is preferred, or at the UE side otherwise.)

values in Tab. III are based on simulations in [8] that enable reliable detection with an overhead of  $T_{\text{sig}}/T_{\text{per}}$  of 5%. Now, the scanning for the synchronization signal for each SCell-UE direction will require  $N_{\text{SCell}}N_{\text{UE}}/L$  scans, where  $L$  is the number of directions in which the receiver can look at any one time. Since there is one scanning opportunity every  $T_{\text{per}}$  s, the total delay is

$$D = \frac{N_{\text{SCell}}N_{\text{UE}}T_{\text{per}}}{L}. \quad (9)$$

The value of  $L$  depends on the beamforming capabilities (and the array size). In the uplink-based design,  $L = 1$  if the SCell receiver has analog BF and  $L = N_{\text{SCell}}$  if it has a fully digital transceiver. Similarly, in the downlink,  $L = 1$  if the UE receiver has analog BF and  $L = N_{\text{UE}}$  if it has a fully digital transceiver. Tab. IV compares the resulting delays for UL- and DL-based designs depending on the BF capabilities of the receiver. We see that the UL design offers a significantly reduced access delay when a digital architecture is preferred and makes it possible to complete every repetition of the measurement reporting framework every at least 1.6 ms (when considering an overhead  $\phi_{\text{ov}} = 5\%$ ). The main reason is that we usually consider  $N_{\text{SCell}} \gg N_{\text{UE}}$ , due to the base station's less demanding space constraints with respect to a mobile terminal: a larger number of antenna elements can be packed at the eNB side, with a consequently number of directions that can potentially be scanned simultaneously through a digital beamforming scheme.

**Rate.** In Tab. V, we evaluate the average rate  $\mathbb{E}[R]$  experienced by a test user when either a multi-connectivity or a traditional standalone mobility management framework is applied, for different SCell density values. It can be observed that the rate achievable with the first solution is higher than with the second one. The reason is that, when relying on the LTE eNB for dealing with outage events, the UE experiences a non-zero throughput, in contrast to the

Tab. V: Rate  $\mathbb{E}[R]$  experienced when either the multi-connectivity framework described in Sec. II or a standalone approach is used.  $T_H = 100$  ms,  $T_{RT} = 300$  ms.

$M$ [SCell/km <sup>2</sup> ]	Multi-connectivity	Standalone
4	8.19 Mbps	5.5 Mbps
10	41.09 Mbps	35.4 Mbps
20	122.9 Mbps	121 Mbps
40	360.42 Mbps	357.6 Mbps
70	778.87 Mbps	777.4 Mbps
90	1103.6 Mbps	1103.6 Mbps

Tab. VI:  $E_C$  to complete each iteration of either the uplink multi-connectivity measurement framework described in Sec. II or a traditional downlink standalone approach. A digital BF configuration is applied at the receiver side.

$T_{\text{per}} = 200 \mu\text{s}$ ,  $N_{\text{SCell}} = 16$  and  $N_{\text{UE}} = 8$ .

Network Entity	UL Scheme UEs transmit SCells receive	DL Scheme UEs receive SCells transmit
SCell	1.7477 J	0.0665 J
UE	0.0287 J	0.8739 J

standalone configuration which cannot properly react to a situation where no mmWave SCells are within reach. The gap between the two architectures is quite remarkable when considering very sparse environments (i.e.,  $M < 20$  SCell/km<sup>2</sup>). In those scenarios, most users would be in an outage pathloss status, making the fallback to the legacy connectivity a vital option to recover a sustainable communication quality. However, achievable rates at those densities are very low due to the quite reduced data rate that a low-bandwidth, overloaded LTE eNB can offer.

We notice that  $\mathbb{E}[R]$  increases with the SCell density  $M$ . In fact, the inter-cell distance is reduced and each UE generally finds a closer SCell (showing better channel propagation conditions) to associate with, thus experiencing an increased SINR (and rate) too. No rate difference is registered between the multi-connectivity and the standalone configurations when considering very dense environments. In those circumstances, users will not suffer an outage and their traffic will be properly handled by the available mmWave SCells, without necessarily having to fallback to the LTE eNB.

Finally, rate gains will likely be even more significant for increasing values of  $T_{RT}$ . In fact, less frequent tracking operations might lead to a more remarkable channel degradation between the transmitter and the receiver, making the fallback to LTE an increasingly attractive option to restore an adequate communication quality.

**Energy Consumption.** The energy consumption ( $E_C$ ) of each mobility management configuration can be evaluated as the product between the power ( $P_C$ ) and the time delay ( $D$ ) required

to complete each iteration of each approach <sup>6</sup>. According to Tab. IV, when considering an uplink multi-connectivity scheme, digital BF is used at the SCell side while analog BF is preferred at the UE side, and  $D^{\text{MC}} = 1.6$  ms. Therefore:

$$E_{C,\text{SCell}}^{\text{MC}} = P_C^{\text{DBF}} \cdot D^{\text{MC}} \quad E_{C,\text{UE}}^{\text{MC}} = P_C^{\text{ABF}} \cdot D^{\text{MC}} \quad (10)$$

For a downlink standalone configuration, analog BF is used at the SCell side while digital BF is preferred at the UE side, and  $D^{\text{SA}} = 3.2$  ms. Therefore

$$E_{C,\text{SCell}}^{\text{SA}} = P_C^{\text{ABF}} \cdot D^{\text{SA}} \quad E_{C,\text{UE}}^{\text{SA}} = P_C^{\text{DBF}} \cdot D^{\text{SA}} \quad (11)$$

In Tab. VI, we compare the energy performance of the two approaches. It is evident that, although the UL scheme is more consuming at the SCell side, it is more energy efficient at the UE side. This represents a very relevant feature of the proposed multi-connectivity framework since mobile terminals are the most *energy-constrained* network entities, due to their limited battery capacity (contrary to the infrastructure nodes which are always power connected and do not suffer from strict energy requirements). We therefore claim that an UL framework, able to reduce the energy consumption of the mobile terminal by around 30 times (with the settings of Tab. VI) with respect to its DL counterpart, should therefore be preferred to enable a more efficient mobility management scheme.

**Robustness.** In order to compare the robustness of the multi-connectivity and the standalone configurations, following the analysis we proposed in [18], we use the ratio

$$R_{\text{var}} = \frac{\sigma_R}{\mathbb{E}[R]}, \quad (12)$$

where  $\mathbb{E}[R]$  is the mean value of the throughput measured for each approach and  $\sigma_R$  is its standard deviation. High values of  $R_{\text{var}}$  reflect remarkable channel instability, thus the rate would be affected by local variations and periodic degradations.

Let  $R_{\text{var}}^{\text{MC}}$  and  $R_{\text{var}}^{\text{SA}}$  be the variance ratios of Eq. (12) for the multi-connectivity and the standalone configurations, respectively. From Fig. 4, we observe that  $R_{\text{var}}^{\text{MC}}$  is lower than  $R_{\text{var}}^{\text{SA}}$ , for each value of density  $M$ , making it clear that the LTE eNB employed in a MC configuration can stabilize the rate, which is not subject to significant variations. In fact, in the portion of time in which the UE would experience zero gain if a standalone architecture were implemented

<sup>6</sup>The total power consumption ( $P_C$ ) of each beamforming scheme is evaluated according to [42], [43], in which  $b = 3$  quantization bits are used by the Analog-to-Digital Converter block.

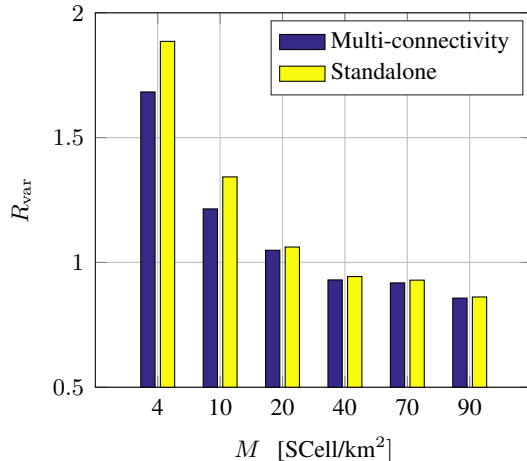


Fig. 4: Average ratio  $R_{\text{var}}$  vs. SCell density, showing the stability of the channel during the simulation.

(due to an outage event), the rate would suffer a noticeable discrepancy with respect to the LoS values, thus increasing the rate variance throughout the simulation. This is not the case for the MC configuration, in which the UE can always be supported by the LTE eNB, even when a blockage event affects the scenario. This result is fundamental for real-time applications, which require a long-term stable throughput to support high data rates and a consistently acceptable Quality of Experience for the users.

Finally, we observe that, in general, the stability of the network rate increases with  $M$  (showing smaller values of  $R_{\text{var}}$ ), due to the more comparable values of SINR (and rate) that are guaranteed. Furthermore, in denser environments and as the probability of pathloss outage decreases, the gap between the two configurations decreases, as the role of the LTE eNB becomes less relevant.

### B. Handover Performance

The test user moves at a constant speed  $v = 20$  m/s towards a specific direction. Due to its motion and to the variability of the mmWave channel over time, it needs to periodically handover or switch its transmitting beam, to recover a good communication quality. The large scale fading parameters of the channel are updated every  $T_H$  s, while the small scale fading parameters are constantly updated every time slot. When building a new CRT every  $T_{\text{RT}}$  s, the MCell can select, by looking at the best saved entry, the new serving SCell for the UE, or just select the new beam pair the transceiver has to set, in order to maximize the communication throughput. We just consider the case  $T_{\text{RT}} \geq T_H$ , as otherwise the rate would almost be constant for all values



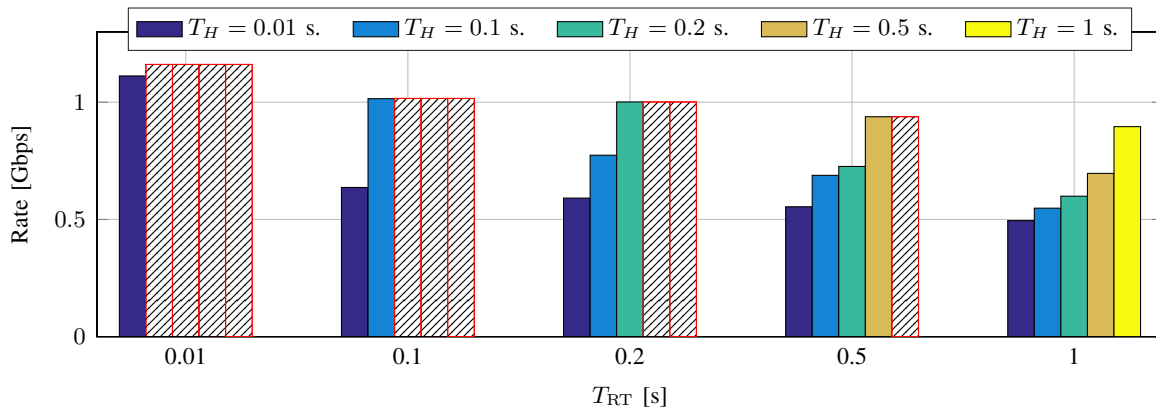


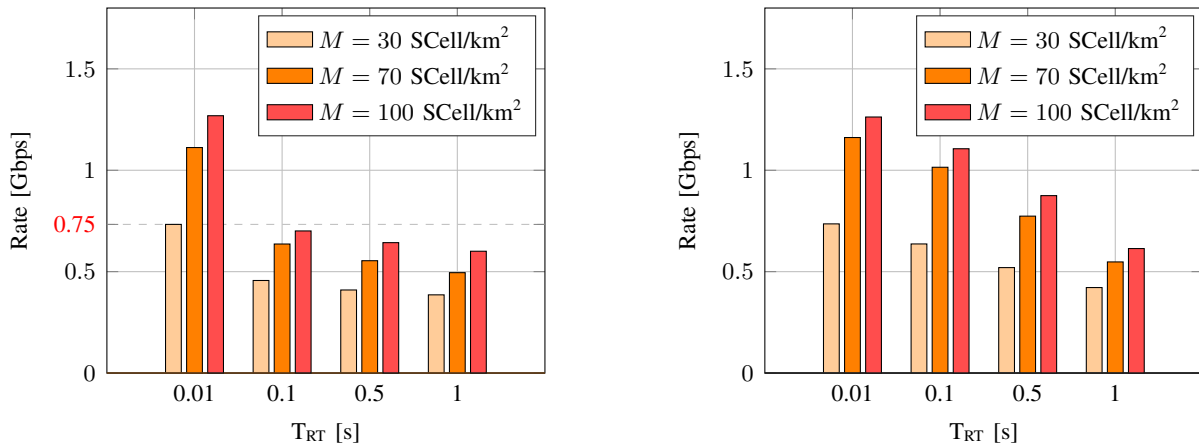
Fig. 5: Average rate vs. RT periodicity  $T_{RT}$ , for different values of  $T_H$ . The mmWave SCell density is kept constant at  $M = 70$  SCell/km<sup>2</sup>. White bars are referred to not remarkable cases, since  $T_{RT} < T_H$ . The user's speed is  $v = 20$  s.

of  $T_H$  (since the beam pair would be updated before the channel even changes its large scale fading parameters).

According to Fig. 5, when  $T_{RT}$  increases, the average rate decreases, since fewer RTs are exchanged and the beam pair between the user and its serving SCell is monitored less frequently. This means that, when the channel changes (due to a pathloss condition modification or to an adaptation of the propagation characteristics) or when the user misaligns with its SCell (due to its motion), the communication quality is not immediately recovered and the throughput is affected by portions of time where suboptimal network settings are chosen. We also observe that, when  $T_H$  increases, the average rate also increases since the channel varies less rapidly, so the rate can assume more stable values even if the SCell-UE beam pair is monitored less frequently. In fact, even if a change in the  $\mathbf{H}$  matrix's large scale fading parameters represents the strongest cause for the user's rate slump, if we consider flat and stable channels, we can accept more rare report tables (and consequently trigger more rare handover and beam switch operations) and still provide sufficiently good communication quality values.

According to Fig. 6 and as we pointed out previously, the average rate increases for increasing mmWave SCell density values. Moreover, higher rates are experienced when  $T_H = 100$  ms (Fig. 6(b)), with respect to the 10 ms case, since the channel changes less rapidly. Additionally, if we observe Fig. 6(a), we note how a 0.75 Gbps rate can be achieved either with a 30 SCell/km<sup>2</sup> density and 10 ms  $T_{RT}$ , or with a 100 SCell/km<sup>2</sup> density and 100 ms  $T_{RT}$ : the tradeoff oscillates between infrastructure cost and signaling overhead.

Finally, it is interesting to notice that the main advantage when increasing the cell density



(a) Average rate vs. RT periodicity  $T_{RT}$ . The large scale fading parameters of  $\mathbf{H}$  are updated every  $T_H = 10$  ms.

(b) Average rate vs. RT periodicity  $T_{RT}$ . The large scale fading parameters of  $\mathbf{H}$  are updated every  $T_H = 100$  ms.

Fig. 6: Results of the handover and beam tracking simulations, for different SCell densities. The user's speed is  $v = 20$  /s.

is observed from  $M = 30$  SCell/km<sup>2</sup> to  $M = 70$  SCell/km<sup>2</sup>. In fact such rate gain reflects the transition from a user outage regime to a LoS/NLoS regime while, as we persistently keep on densifying the network, the deployment of more SCells leads to a considerable increase of the system complexity, while providing a limited increase of the rate.

### C. Initial Access Performance

As assessed in Sec. V-A, faster attachment decisions can be made when an uplink multi-connectivity configuration is preferred. This result enables a faster initial access scheme too, when digital beamforming is chosen. We also claim that the use of the supervising 4G-LTE MCell enables a more fair cell selection operation as well. Unlike in the traditional approach, a multi-connectivity initial access procedure possibly provides the user two different attachment policies: the UE may thus connect (i) to the SCell guaranteeing the highest SINR (max-SNR rule) or, knowing the current load of each eNB, (ii) to the SCell ensuring the highest rate (max-rate rule).

In order to compare the two presented attachment policies, we use *Jain's fairness index*, which is used to determine whether users are receiving a fair share of the system resources and are thus experiencing a rate comparable to that of other users in the cellular system. This index is defined as:

$$J = \frac{\left(\sum_{i=1}^N R_i\right)^2}{N \sum_{i=1}^N R_i^2}, \quad (13)$$

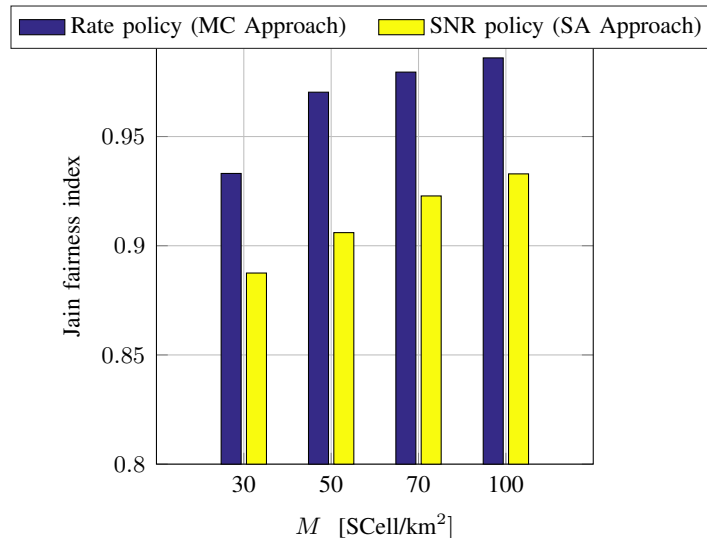


Fig. 7: Jain's fairness index of the rate vs. SCell density, for the initial access procedure. Users within an area of radius  $R_C = 70$  m attach to their best SCell according to a maximum rate or maximum SINR policy.

where  $N$  is the number of users in the system and  $R_i$  is the rate experienced by the  $i$ -th user. The result ranges from  $1/N$  (worst case) to 1 (best case), and it is maximum when all users receive the same allocation.

In Fig. 7, we plot Jain's fairness index for the rate experienced by users within an area of radius  $R_C = 70$  meters, when attaching either according to the max-SINR rule (as in traditional schemes) or the max-rate rule (by exploiting the MC procedure). As expected, this last attachment policy provides higher fairness to the network: asymptotically, a UE accessing the network at time  $t$  will likely find all the SCells in the same load conditions, guaranteeing comparable rates. On the other hand, by following a max-SINR attachment policy, users will tend to connect to the same SCells showing the instantaneous highest signal strengths (and thus overloading them), and avoiding instead nodes that provide lower SINR values (but possibly higher rates, due to their low traffic loads).

We finally notice that Jain's fairness index in Fig. 7 increases with  $M$  for both schemes. In fact, when densifying the network, the SCells ensure more similar propagation conditions to the users, which in turn experience more balanced SINR (and rate) values.

#### D. RLF Recovery Performance

According to the scenario described in Sec. III-C, we define  $R$  as the optimal rate experienced when no obstacles affect the signal propagation, and  $r$  as the suboptimal rate experienced when

a suboptimal backup beam pair is selected, after the primary path is obstructed.

Assume that a blockage event is detected at time  $T_{\text{arr}} \sim \mathcal{U}(0, T_{\text{RT}}) = T_{\text{RT}}p$ , with  $p \in (0, 1)$ , and lasts for  $T_B$  s. We aim at finding the *rate gain* ( $R_G$ ), namely the ratio between the rate experienced when the MC procedure is employed to establish a backup beam pair between the user and its serving SCell after a blockage is detected ( $R_{\text{WB}}$ ), and the rate perceived when no actions are taken ( $R_{\text{OB}}$ ).

We focus on the situation in which the obstacle is no longer present when the new CRT is generated ( $T_{\text{RT}} \geq 2T_B$ ), otherwise the beam pair would be updated when the obstacle is still obstructing the best path, thus still reducing the average rate. Then, the rate  $R_{\text{WB}}$  experienced when reacting after the blockage is detected by selecting a suboptimal solution in the RT instances can be computed (for a fixed time window  $T_{\text{RT}}$ ), as:

$$R_{\text{WB}} = \frac{RT_{\text{arr}} + rT_B + R(T_{\text{RT}} - T_{\text{arr}} - T_B)}{T_{\text{RT}}} = \dots = \frac{R(T_{\text{RT}} - T_B) + rT_B}{T_{\text{RT}}} \quad (14)$$

If no actions are taken, after the obstacle has been detected, the rate  $R_{\text{OB}}$  is:

$$R_{\text{OB}} = \frac{RT_{\text{arr}} + 0T_B + R(T_{\text{RT}} - T_{\text{arr}} - T_B)}{T_{\text{RT}}} = \dots = \frac{R(T_{\text{RT}} - T_B)}{T_{\text{RT}}} \quad (15)$$

The average rate gain ( $R_G$ ) between the two options is:

$$R_G = \frac{R_{\text{WB}}}{R_{\text{OB}}} = 1 + \frac{r}{R} \cdot \frac{T_B}{T_{\text{RT}} - T_B} \quad (16)$$

In Fig. 8, we first notice that  $R_G > 0$  for all values of  $T_{\text{RT}}$  and  $T_B$ , making it clear that having a second available link (in case the primary one is blocked) guarantees improved communication throughput performance with respect to a traditional scheme in which a backup configuration is not available. Furthermore, when  $T_{\text{RT}}$  is sufficiently large, so when  $T_{\text{RT}} \gg 2T_B$ , the simulation curves asymptotically overlap with the dashed lines plotting Eq. (16). Fig. 8 shows also that, for a fixed blockage duration  $T_B$ , as  $T_{\text{RT}}$  increases, the rate gain  $R_G$  decreases. In fact the portion of time in which the user would experience zero gain (if no actions are taken when the primary path is obstructed) proportionally decreases within the time window of length  $T_{\text{RT}}$ , making it less convenient to select a backup beam pair to overcome the blockage issue.

Finally, we see that, when  $T_B$  increases, the rate gain  $R_G$  increases as well, due to the increased enhancement provided by the use of a suboptimal beam pair after a blockage event occurs, with respect to the baseline algorithm in which no actions are taken till the reception of a new CRT.

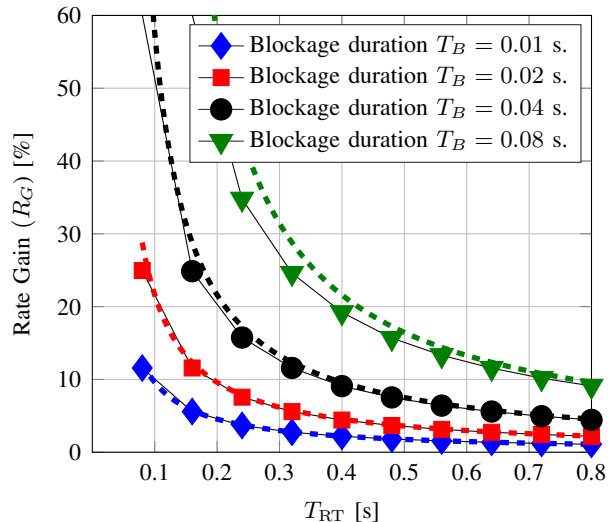


Fig. 8: Rate gain experienced when applying a backup procedure for the RLF recovery vs. RT periodicity  $T_{RT}$ , for different blockage scenarios. The obstacle duration is  $T_B$  s and is detected after  $T_{arr}$  s.

### E. Final Comments

To sum up, a comparison between the uplink multi-connectivity framework presented in this work and a traditional downlink standalone approach has been made. Specifically, we concluded that a MC scheme:

- (i) offers significantly reduced access delays when a digital beamforming architecture is chosen;
- (ii) leveraging on the LTE eNB to deal with outage events, guarantees higher average data rates to the system, especially when considering sparse environments;
- (iii) enables an energy-efficient mobility management scheme for the mobile terminal, the most energy-constrained entity in the cellular network;
- (iv) stabilizes the rate and flattens most of the variations and fluctuations a mmWave channel is usually affected by, improving the performance of real-time applications requiring a long-term stable throughput.

Furthermore, we proved that the proposed framework enables the design of efficient 5G control plane applications that specify how a user should attach to the network and maintain its connectivity. In particular, we showed that a multi-connectivity approach:

- (i) enables performing mobility management operations even when considering highly dynamic environments;
- (ii) enables fast and fair initial access operations, if a max-rate attachment policy is chosen;

- (iii) guarantees an efficient radio-link failure recovery when a backup steering direction is set, in case the primary path is obstructed.

## VI. CONCLUSIONS AND FUTURE WORK

A challenge for the feasibility of a 5G mmWave system is the high susceptibility to the rapid channel dynamics that affect a mmWave environment. In order to deal with these channel variations, a periodic directional sweep should be performed, to constantly monitor the directions of transmission of each potential link and to adapt the beam steering when a power signal drop is detected. In this work, we have presented a measurement reporting system that allows a supervising centralized entity, such as a base station operating in the legacy band, to periodically collect multiple reports on the overall channel propagation conditions, to enable efficient scheduling and mobility management decisions. We argue that the proposed uplink multi-connectivity approach enables more rapid, robust, performing and energy efficient network operations at the mobile terminal, in particular when considering very unstable channels and highly populated systems. Moreover, we proved that fast and fair initial user association, enhanced handover management and reactive radio-link failure recovery can be guaranteed when a multi-connectivity configuration is preferred.

As part of our future work, we will design control applications that monitor and keep memory of the received signal strength variance, to better capture the dynamics of the channel and bias the cell selection strategy of delay-sensitive applications towards more robust cells.

## REFERENCES

- [1] M. Giordani, M. Mezzavilla, S. Rangan, and M. Zorzi, "Multi-Connectivity in 5G mmwave cellular networks," in *15th Annual Mediterranean Ad Hoc Networking Workshop (Med-Hoc-Net'16)*, Vilanova i la Geltru, Barcelona, Spain, Jun. 2016.
- [2] S. Rangan, T. S. Rappaport, and E. Erkip, "Millimeter-wave cellular wireless networks: Potentials and challenges," *Proceedings of the IEEE*, vol. 102, no. 3, pp. 366–385, March 2014.
- [3] M. R. Akdeniz, Y. Liu, M. K. Samimi, S. Sun, S. Rangan, T. S. Rappaport, and E. Erkip, "Millimeter wave channel modeling and cellular capacity evaluation," *IEEE Journal on Selected Areas in Communications*, vol. 32, no. 6, pp. 1164–1179, June 2014.
- [4] J. Lu, D. Steinbach, P. Cabrol, and P. Pietraski, "Modeling the impact of human blockers in millimeter wave radio links," *ZTE Commun. Mag.*, vol. 10, no. 4, pp. 23–28, 2012.
- [5] F. B. Tesema, A. Awada, I. Viering, M. Simsek, and G. P. Fettweis, "Mobility modeling and performance evaluation of multi-connectivity in 5G intra-frequency networks," in *IEEE Globecom Workshops (GC Wkshps)*, Dec 2015.
- [6] Ericsson, *Microwave Towards 2020*, Sep 2015, Report. [Online]. Available: <http://www.ericsson.com/res/docs/2015/microwave-2020-report.pdf>

- [7] K. Haneda, L. Tian, H. Asplund, J. Li, Y. Wang, D. Steer, C. Li, T. Balercia, S. Lee, Y. Kim, A. Ghosh, T. Thomas, T. Nakamura, Y. Kakishima, T. Imai, H. Papadopoulos, T. S. Rappaport, G. R. MacCartney, M. K. Samimi, S. Sun, O. Koymen, S. Hur, J. Park, J. Zhang, E. Mellios, A. F. Molisch, S. S. Ghassamzadeh, and A. Ghosh, "Indoor 5G 3GPP-like channel models for office and shopping mall environments," in *IEEE International Conference on Communications Workshops (ICC)*, May 2016, pp. 694–699.
- [8] C. N. Barati, S. A. Hosseini, M. Mezzavilla, P. Amiri-Eliasi, S. Rangan, T. Korakis, S. S. Panwar, and M. Zorzi, "Directional initial access for millimeter wave cellular systems," in *49th Asilomar Conference on Signals, Systems and Computers*, Nov 2015, pp. 307–311, *CoRR*, vol. abs/1511.06483. [Online]. Available: <http://arxiv.org/abs/1511.06483>
- [9] M. Giordani, M. Mezzavilla, A. Dhananjay, S. Rangan, and M. Zorzi, "Channel dynamics and SNR tracking in millimeter wave cellular systems," in *European Wireless 2016 (EW2016)*, Oulu, Finland, May 2016, pp. 306–313.
- [10] M. Giordani, M. Mezzavilla, and M. Zorzi, "Initial access in 5G mmWave cellular networks," *IEEE Communications Magazine*, vol. 54, no. 11, pp. 40–47, November 2016.
- [11] R. Irmer, H. Droste, P. Marsch, M. Grieger, G. Fettweis, S. Brueck, H. P. Mayer, L. Thiele, and V. Jungnickel, "Coordinated multipoint: Concepts, performance, and field trial results," *IEEE Communications Magazine*, vol. 49, no. 2, pp. 102–111, February 2011.
- [12] H. Shokri-Ghadikolaei, C. Fischione, G. Fodor, P. Popovski, and M. Zorzi, "Millimeter wave cellular networks: A MAC layer perspective," *IEEE Transactions on Communications*, vol. 63, no. 10, pp. 3437–3458, Oct 2015.
- [13] S. Schwarz, C. Mehlführer, and M. Rupp, "Calculation of the spatial preprocessing and link adaption feedback for 3GPP UMTS/LTE," in *Proc. IEEE Conf. Wireless Advanced (WiAD)*. IEEE, 2010.
- [14] 3GPP, "Technical specification group radio access network; Study on small cell enhancement for (E-UTRA) and (e-TRAN); Higher layer aspects (Release 12)," *TR 36.842*, 2013.
- [15] A. Zakrzewska, D. Lopez-Perez, S. Kucera, and H. Claussen, "Dual connectivity in LTE HetNets with split control- and user-plane," in *IEEE Globecom Workshops (GC Wkshps)*, Dec 2013, pp. 391–396.
- [16] Z. He, S. Mao, and T. S. Rappaport, "Minimum time length link scheduling under blockage and interference in 60 GHz networks," in *IEEE Wireless Communications and Networking Conference (WCNC)*, March 2015, pp. 837–842.
- [17] V. Yazici, U. C. Kozat, and M. O. Sunay, "A new control plane for 5G network architecture with a case study on unified handoff, mobility, and routing management," *IEEE Communications Magazine*, vol. 52, no. 11, pp. 76–85, Nov 2014.
- [18] M. Polese, M. Giordani, M. Mezzavilla, S. Rangan, and M. Zorzi, "Improved handover through dual connectivity in 5G mmWave mobile networks," *to appear in the 2017 IEEE JSAC Special Issue on Millimeter Wave Communications for Future Mobile Networks*, 2017. [Online]. Available: <http://arxiv.org/abs/1611.04748>
- [19] M. Giordani, A. Zanella, and M. Zorzi, "Millimeter wave communication in vehicular networks: Challenges and opportunities," in *6th International Conference on Modern Circuits and Systems Technologies (MOCASST)*, May 2017.
- [20] S. Sesia, I. Toufik, and M. Baker, *The UMTS Long Term Evolution: From Theory to Practice*. Wiley Publishing, 2009.
- [21] X. Yan, Y. A. Sekercioglu, and S. Narayanan, "A survey of vertical handover decision algorithms in Fourth Generation heterogeneous wireless networks," *Computer Networks*, vol. 54, no. 11, pp. 1848 – 1863, 2010. [Online]. Available: <http://www.sciencedirect.com/science/article/pii/S1389128610000502>
- [22] M. Kuhnert and C. Wietfeld, "Performance evaluation of an advanced energy-aware client-based handover solution in heterogeneous lte and wifi networks," in *2014 IEEE 79th Vehicular Technology Conference (VTC Spring)*, May 2014.
- [23] A. Talukdar, M. Cudak, and A. Ghosh, "Handoff rates for millimeterwave 5G systems," in *IEEE 79th Vehicular Technology Conference (VTC Spring)*, May 2014.
- [24] H. Song, X. Fang, and L. Yan, "Handover scheme for 5G C/U plane split heterogeneous network in high-speed railway," *IEEE Transactions on Vehicular Technology*, vol. 63, no. 9, pp. 4633–4646, Nov 2014.

- [25] S. Sadr and R. S. Adve, "Handoff rate and coverage analysis in multi-tier heterogeneous networks," *IEEE Transactions on Wireless Communications*, vol. 14, no. 5, pp. 2626–2638, May 2015.
- [26] P. Coucheney, E. Hyon, and J. M. Kelif, "Mobile association problem in heterogenous wireless networks with mobility," in *IEEE 24th Annual International Symposium on Personal, Indoor, and Mobile Radio Communications (PIMRC)*, Sept 2013, pp. 3129–3133.
- [27] M. Giordani, M. Mezzavilla, N. Barati, S. Rangan, and M. Zorzi, "Comparative analysis of initial access techniques in 5G mmwave cellular networks," in *Annual Conference on Information Science and Systems (CISS)*, Princeton, USA, 2016.
- [28] C. N. Barati, S. A. Hosseini, S. Rangan, P. Liu, T. Korakis, S. S. Panwar, and T. S. Rappaport, "Directional cell discovery in millimeter wave cellular networks," *IEEE Transactions on Wireless Communications*, Dec 2015.
- [29] A. Capone, I. Filippini, and V. Sciancalepore, "Context information for fast cell discovery in mm-Wave 5G networks," in *Proceedings of 21th European Wireless Conference*, May 2015.
- [30] V. Desai, L. Krzymien, P. Sartori, W. Xiao, A. Soong, and A. Alkhateeb, "Initial beamforming for mmWave communications," in *48th Asilomar Conference on Signals, Systems and Computers*, Nov 2014, pp. 1926–1930.
- [31] T. S. Rappaport, R. W. Heath Jr, R. C. Daniels, and J. N. Murdock, *Millimeter wave wireless communications*. Pearson Education, 2014.
- [32] N. Moraitis and P. Constantinou, "Indoor channel measurements and characterization at 60 GHz for wireless local area network applications," *IEEE Transactions on Antennas and Propagation*, vol. 52, no. 12, pp. 3180–3189, Dec 2004.
- [33] T. Nitsche, A. B. Flores, E. W. Knightly, and J. Widmer, "Steering with eyes closed: Mm-wave beam steering without in-band measurement," in *IEEE Conference on Computer Communications (INFOCOM)*, April 2015, pp. 2416–2424.
- [34] A. Patra, L. Simic, and P. Mahonen, "Smart mm-wave beam steering algorithm for fast link re-establishment under node mobility in 60 GHz indoor WLANs," in *MobiWac*, 2015, pp. 53–62.
- [35] S. Ferrante, T. Deng, R. Pragada, and D. Cohen, "mmWave initial cell search analysis under UE rotational motion," in *IEEE International Conference on Ubiquitous Wireless Broadband (ICUWB)*, Oct 2015.
- [36] T. S. Rappaport, G. R. MacCartney, M. K. Samimi, and S. Sun, "Wideband millimeter-wave propagation measurements and channel models for future wireless communication system design," *IEEE Transactions on Communications*, vol. 63, no. 9, pp. 3029–3056, Sept 2015.
- [37] M. K. Samimi and T. S. Rappaport, "3-D statistical channel model for millimeter-wave outdoor mobile broadband communications," in *Proc. ICC*, June 2015, pp. 2430–2436.
- [38] S. Sun, T. S. Rappaport, R. W. Heath, A. Nix, and S. Rangan, "MIMO for millimeter-wave wireless communications: Beamforming, spatial multiplexing, or both?" *IEEE Communications Magazine*, vol. 52, no. 12, pp. 110–121, 2014.
- [39] T. Bai and R. W. Heath, "Coverage and rate analysis for millimeter-wave cellular networks," *IEEE Transactions on Wireless Communications*, vol. 14, no. 2, pp. 1100–1114, Feb 2015.
- [40] 3GPP, "Technical specification group radio access network; study on scenarios and requirements for next generation access technologies (Release 14)," *TR 38.913*, 2017.
- [41] K. Chandra, R. V. Prasad, I. G. Niemegeers, and A. R. Biswas, "Adaptive beamwidth selection for contention based access periods in millimeter wave WLANs," in *IEEE 11th Consumer Communications and Networking Conference (CCNC)*. IEEE, 2014, pp. 458–464.
- [42] W. B. Abbas and M. Zorzi, "Towards an appropriate receiver beamforming scheme for millimeter wave communication: A power consumption based comparison," in *22th European Wireless Conference*, May 2016.
- [43] —, "Towards an appropriate beamforming scheme for initial cell discovery in mmW 5G cellular networks," in *arXiv preprint arXiv:1605.00508*, 2016.